Materials Science in Semiconductor Processing 102 (2019) 104595

Contents lists available at ScienceDirect

Materials Science in Semiconductor Processing

journal homepage: www.elsevier.com/locate/mssp

Morphological, structural and optical properties of Mg-doped ZnO nanocrystals synthesized using polyol process

Oleksandr Dobrozhan[a,b,*], Oleksii Diachenko[a], Maksym Kolesnyk[a], Andriy Stepanenko[a], Serhii Vorobiov[c], Peter Baláž[b], Sergei Plotnikov[d], Anatoliy Opanasyuk[a]

[a] Department of Electronics and Computer Technology, Sumy State University, Sumy, Ukraine
[b] Department of Mechanochemistry, Institute of Geotechnics, Slovak Academy of Sciences, Košice, Slovakia
[c] Institute of Physics, P.J. Šafárik University in Košice, Košice, Slovakia
[d] East Kazakhstan State Technical University, Ust-Kamenogorsk, Kazakhstan

ARTICLE INFO

Keywords:
Zinc oxide nanocrystals
Magnesium doping
Polyol process
Morphology
Structure
Optical properties

ABSTRACT

In this work, the undoped and Mg (0.5–20.0 at.%) doped ZnO nanocrystals have been synthesized using the polyol process and their morphological, structural, optical properties as well as chemical composition have been investigated. X-ray diffraction, transmission and scanning electron microscopy, energy dispersive X-ray, Raman and UV-vis spectroscopies were used to identify effective incorporation of Mg atoms into ZnO lattice without the formation of secondary phases at Mg up to 5 at.%. At higher Mg doping level, $Mg(OH)_2$ phase traces were evidenced. The results have revealed the reduction of sizes and worsening the crystal quality of ZnO nanocrystals with increase of Mg doping. ZnO nanocrystals lose spherical shape forming the rod-like and amorphous nanostructures at Mg ≥ 5 at.%. Raman spectra have confirmed $E_2^{(high)}$, $E_2^{(low)}$, $E_2^{(high)}$ - $E_2^{(low)}$, A_1(TO) modes for undoped, and E_u(TO) mode for Mg-doped ZnO nanocrystals. The optical band gap has been found in the range of 3.40–3.80 eV.

1. Introduction

In recent years, zinc oxide (ZnO) nanocrystals have become one of the most promising research materials due to its unique properties and possible applications. ZnO is *n*-type semiconductor which has wide bandgap energy (~3.37 eV at 300 K), large exciton binding energy (~60 meV, in comparison ZnSe has only 20 meV) and hexagonal unit cell with lattice constants of $a = b = 0.325$ nm, $c = 0.521$ nm [1]. The great attention has been paid to ZnO nanocrystals due to their ability to show new optical, electrical, chemical and mechanical properties as compared with the bulk form [2,3].

Due to the excellent optoelectronic properties, non-toxicity, natural abundance and low cost, ZnO nanocrystals have already been used in solar cells [4–6], light-emitting diodes [7], thermoelectrics [8], photocatalysis [9], sensors [10] and bioapplications [11,12], among others. In general, chemical approaches to synthesize the nanomaterials are cheaper, faster and provide a higher yield than physical methods allowing the industrial scales for various applications. Literature survey shows that undoped ZnO nanocrystals have been prepared using the different solution-based techniques including polyol process [5,10,13–20], co-precipitation reaction [21], colloidal synthesis [22,23], solvothermal [24] and hydrothermal approaches [25], sol-gel method [26], electrochemical synthesis [27].

It is well known that appropriate doping with various metal atoms, in particular with alkaline earth metals, is an effective strategy to modify the functional properties of ZnO nanocrystals and to modulate their optical and electrical properties [28,29]. Also, it is well-known that nanocrystals possess a high surface to volume ratio which can lead to unstable properties due to the chemisorption of oxygen at the surface at ambient atmosphere that causes the higher resistivity or uncontrolled luminescence emissions. This obstacle can be prevented by the careful passivation of the nanocrystals surface bonds with the appropriate guest atoms thus leading to stable state. The choice of the suitable doping atoms generally relies on the following rules:

- ionic radius of the guest and host atoms should possess the similar values;
- thermodynamic solubility limit should be as high as possible to keep the high content of the guest atoms.

Among the possible doping atoms, magnesium (Mg) ions with the electronic configuration $[Ne]3s^2$ is the promising candidate for the

* Corresponding author. full postal address: 2, Rymskogo-Korsakova st., 40007, Sumy, Ukraine.
E-mail addresses: dobrozhan.a@gmail.com, o.dobrozhan@ekt.sumdu.edu.ua (O. Dobrozhan).

https://doi.org/10.1016/j.mssp.2019.104595
Received 19 March 2019; Received in revised form 9 June 2019; Accepted 26 June 2019

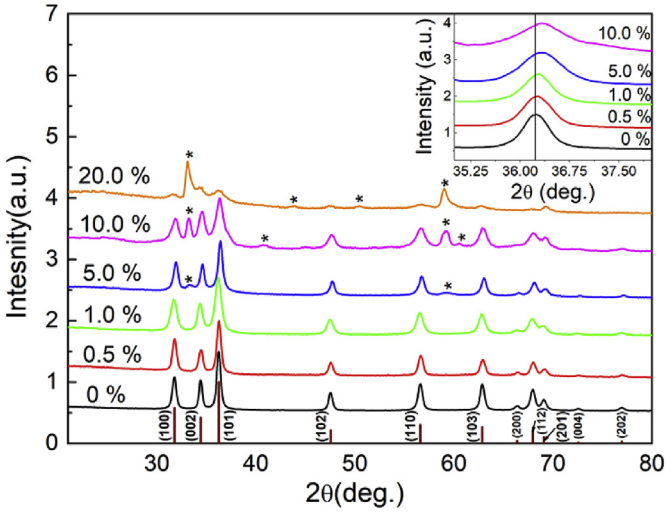

Fig. 1. XRD patterns of undoped and Mg-doped ZnO nanocrystals. The vertical brown lines correspond to JCPDS card # 01-079-2205 of hexagonal ZnO phase. The asterisk symbols show the peaks of secondary $Mg(OH)_2$ phase. The inset shows a detail of (101) peak of ZnO phase at around $2\theta = 36.2^{\circ}$. (For interpretation of the references to colour in this figure legend, the reader is referred to the Web version of this article.)

substitution of Zn sites with the purpose to tune the optical properties (e.g. band gap energies, E_g are in case of MgO, 7.70 eV for bulk materials, and 3.80 eV for thin films [30]) as well as to enhance luminescence emission (e.g. increase the intensity of UV emission) of the host lattice. Moreover, magnesium is well-known as the low toxic and nature abundant element. In addition, Mg ions should not lead to a large lattice distortion due to the similar ionic radius with Zn (corresponding to 0.057 nm for Mg^{2+} and is 0.060 nm for Zn^{2+}) [31].

Furthermore, there is a number of works devoted to the doping of ZnO nanocrystals with Mg alkaline earth ions to substitute the zinc sites in the initial lattice which can be prepared by numbers of solution-based techniques including polyol process [32,33], colloidal synthesis [34], co-precipitation reaction [35,36] and sol-gel method [37–40]. Among solution-based techniques, polyol process is an efficient approach to synthesize ZnO nanocrystals due to its simplicity, cost efficiency and scalability.

There are several valuable reports on morphological, structural and optical properties of ZnO materials. In brief, Abed et al. [41] have obtained porous ZnO with adding Ag inclusions. It was found that ZnO possessed hexagonal wurtzite structure with the change in optical band gap in the range of 2.91–3.06 eV. Another works [42–45] show that hexagonal wurtzite ZnO structures have the preferred orientation growth along c-axis with the crystallite sizes in the nanometer range. The morphological aspects of obtained ZnO structures include the paper-like nanosheets, nanorods, tapered tips, packed and dense particles obtained depending on the preparation conditions.

However, to the best of our knowledges, there are only two works devoted to ZnO nanocrystal doped with Mg ions synthesized using polyol process [32,33]. Herein, we focus our discussion on the morphological, structural, optical properties and chemical composition of Mg-doped ZnO nanocrystals prepared by polyol synthesis. We were looking for the optimal doping level to synthesize the high-quality Mg-doped ZnO nanocrystals with the single crystal structure and tunable band gap energies.

2. Experimental

2.1. Chemicals

All chemicals have been purchased from Sigma Aldrich and used as received: zinc acetate dihydrate ($Zn(CH_3COO)_2{\cdot}2H_2O$, 99.9%), magnesium dichloride ($MgCl_2$, 99.9%), ethylene glycol EG ($C_2H_6O_2$, 90%), isopropanol (C_3H_8O, 90%).

2.2. Synthesis of undoped and Mg-doped ZnO nanocrystals

ZnO nanocrystals have been synthesized through the alcoholysis and condensation reaction, known as polyol process, of Zn $(CH_3COO)_2{\cdot}2H_2O$ (2.2 g) in EG (10 ml) at 160 °C, similar to work [15]. To dope the nanocrystals, $MgCl_2$ was added to the initial reaction with 0, 0.5, 1.0, 5.0, 10.0, 20.0 at.% concentrations. The precipitation of ZnO nanocrystals has occurred after heating up the solution in a round-bottom flask fitted with a reflux condenser for 4 h under magnetic stirring. The nanocrystals have been recovered by the centrifugation and washed once with isopropanol for further characterizations.

2.3. Characterizations

The morphology of nanocrystals was assessed using transmission electron microscopy (TEM, Selmi, Ukraine) and scanning electron microscopy (SEM, Tescan, Czech Republic). Phase analysis was performed using X-ray diffraction (XRD, DRON-4, Russia) with Cu K_α radiation ($\lambda = 0.15406$ nm) operating at 40 kV and 20 mA over a 2θ range of 20–80° as well as applying selected area diffraction (SAED) using TEM. The details of the used methodologies to study the structural properties are well described in our previous works [46,47]. Briefly, the crystallite sizes of synthesized samples have been determined by Scherrer equation [48]:

$$D = \frac{0.9{\cdot}\lambda}{FWHM{\cdot}\cos(\theta)}, \quad (1)$$

where, λ, $FWHM$, θ are X-ray wavelength, full width at half maximum and Bragg diffraction angle.

The lattice constants, a and c, of ZnO crystal lattice have been calculated according to the following equations [49]:

$$a = \frac{\lambda}{2\sin\theta}\sqrt{\frac{4}{3}(h^2 + hk + k^2) + \left(\frac{a}{c}\right)^2 l^2},$$
$$c = \frac{\lambda}{2\sin\theta}\sqrt{\frac{4}{3}\left(\frac{c}{a}\right)^2 (h^2 + hk + k^2) + l^2}, \quad (2)$$

The chemical composition was measured by using energy dispersive

Table 1
The structural parameters of undoped and Mg-doped ZnO nanocrystals. The most intense (101) peak of ZnO phase was chosen for the calculations.

Doping concentration, at.%	$2\theta_{(101)}$, deg	$(I^{doped})/I^{undoped})_{(101)}$, %	FWHM, deg.	$D_{(101)}$, nm	a, nm	c, nm	c/a	V_{unit}, x10^{-3} nm^3
0	36.23	100	0.656	19.1	0.31438	0.50367	1.6021	43.11
0.5	36.26	89	0.710	17.7	0.31463	0.50407	1.6021	43.21
1.0	36.29	88	0.718	17.5	0.31488	0.50448	1.6021	43.32
5.0	36.32	87	0.872	14.4	0.31513	0.50488	1.6021	43.42
10.0	36.33	75	1.044	12.0	0.31521	0.50501	1.6021	43.46
20.0	36.36	25	1.480	8.5	0.31547	0.50542	1.6021	43.56
Reference (JCPDS card # 01-079-2205)	36.25	–	–	–	0.32501	0.52071	1.6021	47.63

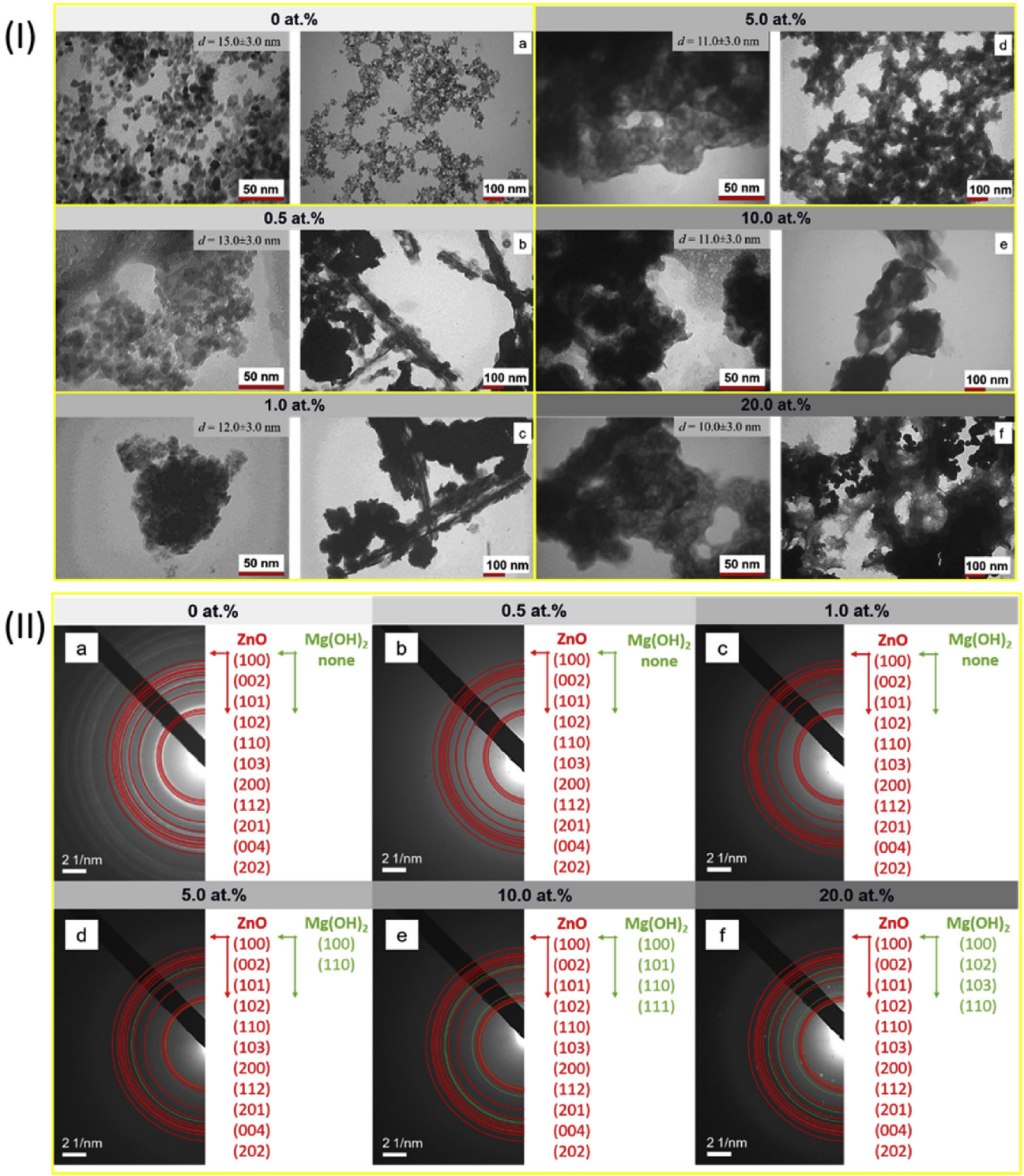

Fig. 2. (I) TEM images and (II) SAED patterns of (a) undoped and (b–f) doped ZnO nanocrystals with the different Mg concentrations: (b) 0.5 at.%, (c) 1.0 at.%, (d) 5.0 at.%, (e) 10.0 at.%, (f) 20.0 at.%.

X-ray spectroscopy (Oxford instrument) operating at 20 keV. The room temperature Raman measurements were performed using a confocal Raman microscope (Horiba-MTB Xplora, Japan). The device was equipped with excitation laser having a wavelength of 532 nm and intensity of 1 mW. The measurements were carried out in the spectral range from 50 up to 800 cm^{-1}. The optical properties of ZnO nanoparticles were investigated using the room temperature optical spectroscopy, Lasany-722 (India) spectrophotometer (instrumental error 1%), in the wavelength range of λ = 350–900 nm. The bandgap energies of ZnO nanocrystals were determined by using the techniques described in detail elsewhere [50,51]. The absorption spectra were calculated using Lambert's equation given by $\alpha = (\ln 100/T)/t$, where T is the transmittance and t is the thickness of used quartz cuvette. Then, values of $(\alpha h\nu)^2$ were plotted against energies ($h\nu$) and linear part of the curve in UV range has been extrapolated to intersect $h\nu$ axis giving the value of optical band gap (E_g) of the synthesized nanocrystals [51].

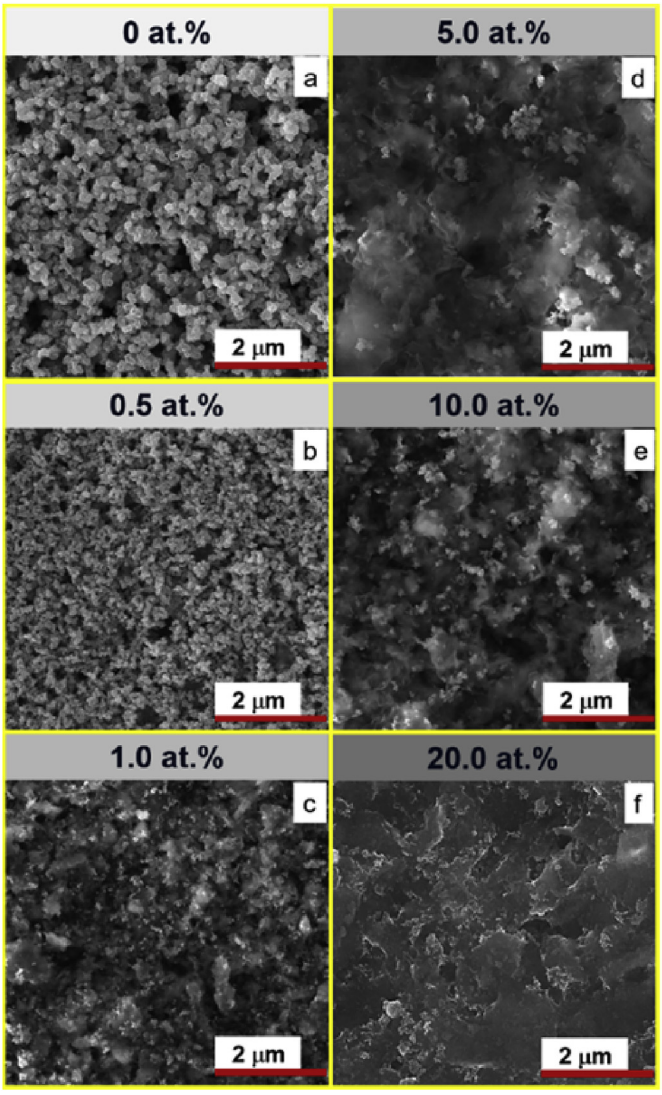

Fig. 3. SEM images of (a) undoped and (b–f) doped ZnO nanocrystals with the different Mg concentrations: (b) 0.5 at.%, (c) 1.0 at.%, (d) 5.0 at.%, (e) 10.0 at.%, (f) 20.0 at.%.

Table 2
The chemical composition analysis of undoped and Mg-doped ZnO nanocrystals.

Doping level, at.%	C_{Zn}, at.%	C_O, at.%	C_{Mg}, at.%	C_{Cl}, at.%	$\gamma_{Zn/O}$ for undoped $\gamma_{(Zn+Mg)/O}$ for doped
0	49.1	50.6	0.0	0.3	0.97
0.5	46.2	53.0	0.5	0.3	0.88
1.0	42.3	56.7	0.8	0.2	0.76
5.0	41.3	57.1	3.4	0.2	0.75
10.0	39.9	58.1	3.7	0.3	0.72
20.0	30.1	66.0	3.6	0.3	0.51

3. Results and discussion

X-ray diffraction patterns of undoped and Mg-doped ZnO nanocrystals are shown in Fig. 1, including the reference pattern of pure hexagonal ZnO phase (brown vertical lines correspond to JCPDS card # 01-079-2205). Up to 1.0 at.%, we have observed a single hexagonal ZnO phase suggesting that no other secondary phases were presented in the nanocrystals. However, further increase in Mg concentration from 5.0 at.% up to 20.0 at.% led to the appearance of the reflections at 32.8°, 40.7°, 43.8°, 50.5°, 58.7°, 60.4° corresponding to hexagonal Mg $(OH)_2$ phase (asterisk symbols, JCPDS card # 00-007-0239). The intensities of three major (100), (002), (101) peaks of ZnO phase decreases and FWHM increases indicating both the worsening of the crystal quality and reduction of ZnO nanocrystals size. This behavior can be explained that Mg atoms may be located at the interfaces or on the surface of ZnO nanoparticles, resulting in decrease of Mg diffusion rate thus preventing the nanocrystal growth.

At the same time, intensities of (100) at 32.8° and (110) at 58.7° 2θ values of $Mg(OH)_2$ phase increases indicating its content increase in the synthesized nanomaterials.

In order to identify the effect of Mg doping on the structural parameters of ZnO nanocrystals, we have determined the crystallite size (D), lattice parameters (a, c, c/a) and cell volume (V_{unit}) of ZnO phase. The results of the calculations are presented in Table 1. The quality of nanocrystals was lowering with the Mg concentration increase. This supports by the decrease of (101) main peak intensity ratio as well as by the FWHM widening.

The calculation of crystallite size of the samples using Scherrer equation [48] shows that Mg amount increase led to the decrease of D from ~19.1 to ~8.5 nm and a very small increase of V_{unit} from ~43.1 to ~43.5 nm.

The doped ZnO nanocrystals were characterized by smaller a and c lattice parameters compared to the values in the bulk ZnO materials as evidenced by a slight peak shift toward higher angles in XRD patterns shown on the inset in Fig. 1. The lattice expansion can be attributed to the substitution of Zn^{2+} (0.060 nm) by slightly smaller Mg^{2+} (0.057 nm) cations [31]. Moreover, there is the reverse relationship between the size and lattice parameters of semiconductor nanocrystals which has been shown by Shreiber et al. [52].

Diehm et al. have also explained such behavior by presence of negative surface stress excluding excess of lattice sums or point defects of charge states [53]. The appearance of the small amount of the secondary phases at 5.0 at.% suggest reaching of thermodynamic solubility limit of Mg in ZnO nanocrystals which is also evidenced by the phase diagram of MgO-ZnO binary system [54].

TEM and SEM images of the synthesized ZnO nanocrystals are presented in Figs. 2–3. Both imaging techniques show particles with the spherical shape and diameter of 15 ± 3 nm for undoped samples. Mg doping leads to a decrease of nanocrystal size (up to 10 ± 3 nm at 20.0 at.%) which is supported by XRD analysis (Fig. 1, Table 1). The quasispherical nanoobjects with a diameter of 40–50 nm appear at 20.0 at.% suggesting the formation of $Mg(OH)_2$ secondary phase as evidenced by XRD and Raman measurements. Besides it, the measured SAED patterns (Fig. 2) confirmed the presence of the secondary Mg $(OH)_2$ phase for samples doped with 5–20 at.% of Mg ions.

At 0.5 at.% doping, the nanocrystals start to lose their spherical shape forming a rod-like and amorphous net with the width of 70–100 nm which also supports XRD analysis results on the worsening the crystal quality of Mg-doped ZnO nanocrystals.

It is worth mentioning that based on XRD, TEM, SEM analyses, we clearly can state that the synthesized ZnO nanocrystals are not in the quantum confinement regime (e.g., excitonic Bohr radius for ZnO is ~3.5 nm [55]) thus isolating the doping influence on the properties of ZnO nanocrystals from quantum confinement effects.

EDS data obtained for both undoped and Mg-doped ZnO nanocrystals indicate the successful incorporation of Mg ions into the host oxide lattice, as can be seen in Table 2 and Fig. 4. EDS elemental mapping (on the example of 1 at.% of Mg atoms) of Zn, O, Mg elements show that the synthesized nanocrystals are composed of Zn and O elements with randomly distributed Mg and small traces of Cl residuals (up to 0.3 at.%) which originates from the initial magnesium dichloride salt used in the polyol process. As can be seen in Table 2, undoped samples possess the high stoichiometry ($\gamma_{Zn/O}$ = 0.97). The increase in Mg doping concentration leads to an increase of the level of magnesium

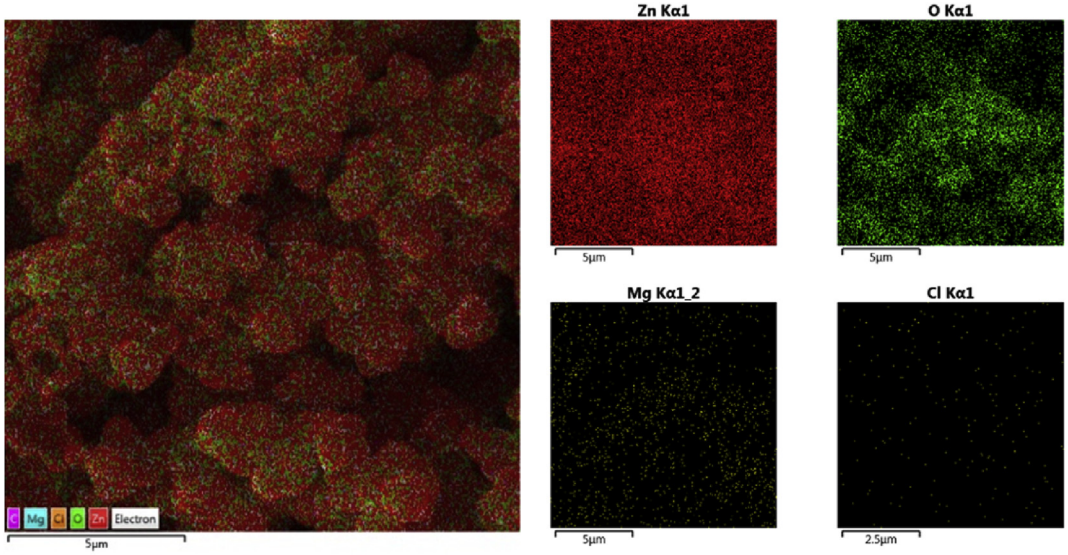

Fig. 4. EDS mapping of Zn, O, Mg, Cl elements in doped ZnO nanocrystals with 1.0 at.% of Mg atoms.

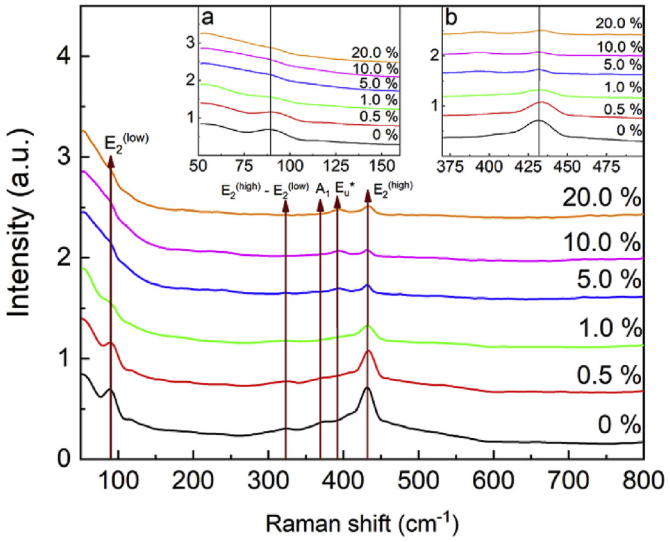

Fig. 5. Raman spectra of undoped and Mg-doped ZnO nanocrystals. Inset (a) and asterisks corresponds to E_u(TO) mode of $Mg(OH)_2$ phase.

incorporation into the host zinc oxide lattice reaching the solubility limit of 4 at.% at the nominal introduced amount of 5–20 at.%. Also, the doping causes the worsening stoichiometry of the synthesized nanocrystals from 0.97 (for undoped sample) to 0.51 (for 20 at.% doped samples).

This can be explained by the appearance of oxygen-related defects at the nanocrystals surface as well as due to formation of secondary O-contained phases as shown by XRD, TEM, SEM measurements. Raman spectroscopy is an effective nondestructive method to evaluate the crystal quality of the nanomaterials and to detect incorporation of dopants or appearance of crystal defects and lattice distortion.

The hexagonal structure of ZnO belongs to the space group C_{6v}^4 having two units per cell. The optical phonons in ZnO unit cell can be described by the equation $\Gamma_{opt} = A_1 + 2B_1 + E_1 + 2E_2$ [56]. A_1 and E_1 modes are Raman and infrared active polar phonons showing the appearance of TO and LO modes. E_2 mode is a non-polar and Raman active showing two frequencies: $E_2^{(high)}$ which is attributed to the oxygen anions and $E_2^{(low)}$ – to the zinc cations in the unit lattice. In addition, B_1 mode is Raman inactive [56].

Fig. 5 shows Raman spectra of undoped and Mg-doped ZnO nanocrystals in the frequency range of 50–800 cm^{-1}. For the synthesized nanocrystals, Raman modes at 89, 323, 370 and 432 cm^{-1} are assigned

Table 3
Raman modes identification and the ratio of the intensities, FWHM of the main $E_2^{(high)}$ mode of undoped and Mg-doped ZnO nanocrystals.

Doping level, at.%	Raman shift in our samples, cm^{-1}	Mode	References	$(I^{doped})/I^{undoped})(E_2^{(high)})$, %	FWHM($E_2^{(high)}$), cm^{-1}
0	89	$E_2^{(low)}$	[14]	100	20.1
	323	$E_2^{(high)}$ - $E_2^{(low)}$	[10,20]		
	370	A_1(TO)	[14,20,40]		
	432	$E_2^{(high)}$	[10,14,20,40]		
0.5	90	$E_2^{(low)}$	[14]	74.8	24.4
	325	$E_2^{(high)}$ - $E_2^{(low)}$	[10,20]		
	434	$E_2^{(high)}$	[10,14,20,40]		
1.0	89	$E_2^{(low)}$	[14]	34.5	25.2
	325	$E_2^{(high)}$ - $E_2^{(low)}$	[10,20]		
	434	$E_2^{(high)}$	[10,14,20,40]		
5.0	90	$E_2^{(low)}$	[14]	20.2	13.6
	393	E_u(TO)-$Mg(OH)_2$	[59,60]		
	434	$E_2^{(high)}$	[10,14,20,40]		
10.0	91	$E_2^{(low)}$	[14]	14.3	14.4
	393	E_u(TO)-$Mg(OH)_2$	[59,60]		
	434	$E_2^{(high)}$	[14,20,40]		
20.0	92	$E_2^{(low)}$	[14]	14.2	15.6
	393	E_u(TO)-$Mg(OH)_2$	[59,60]		
	434	$E_2^{(high)}$	[14,20,40]		

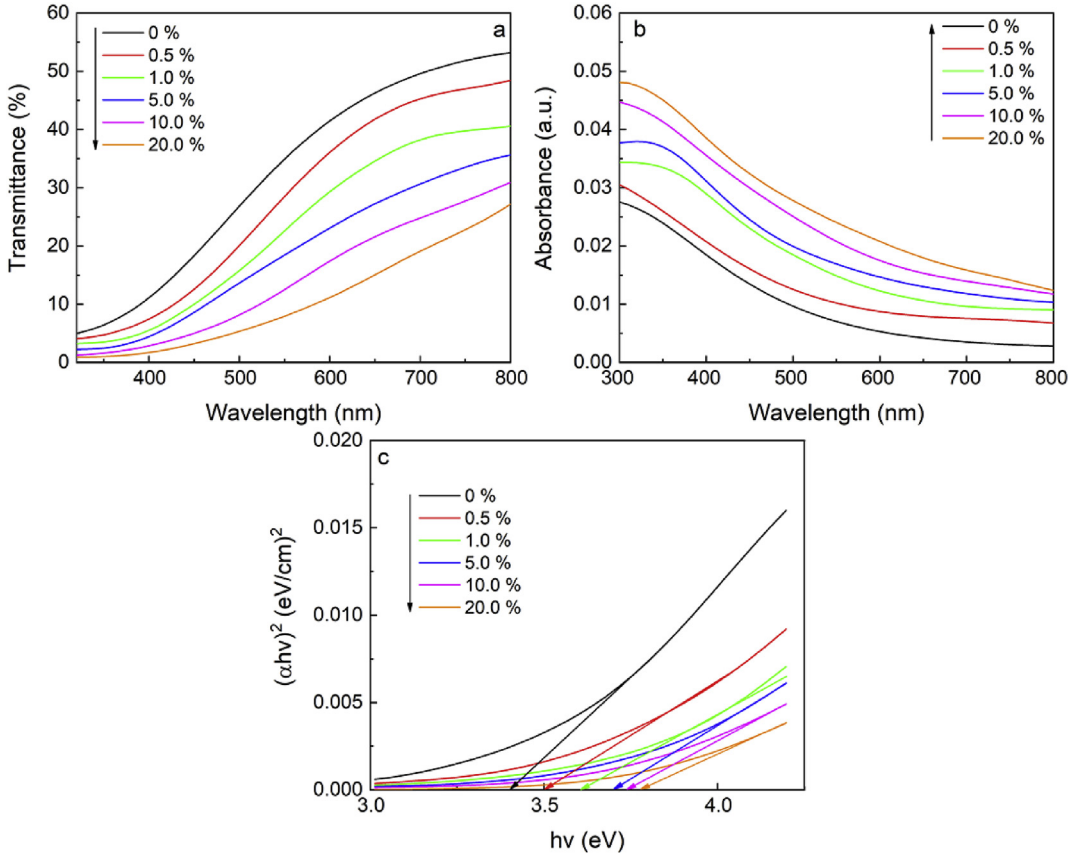

Fig. 6. (a) Transmittance, (b) absorbance spectra of undoped and Mg-doped ZnO nanocrystals and (c) $(\alpha h\nu)^2$-$(h\nu)$ plot for E_g determination.

Table 4
Optical band gap of undoped and Mg-doped ZnO nanocrystals.

Doping level, at.%	E_g, eV
0	3.40 ± 0.034
0.5	3.50 ± 0.035
1.0	3.62 ± 0.036
5.0	3.71 ± 0.037
10.0	3.74 ± 0.037
20.0	3.80 ± 0.038
Reference data for bulk ZnO material	3.37 [1]

to $E_2^{(low)}$, $E_2^{(high)}$ - $E_2^{(low)}$, A_1(TO), $E_2^{(high)}$ modes of the hexagonal ZnO crystal structure, respectively. The highest 432 cm^{-1} ($E_2^{(high)}$) mode, characterizing the hexagonal crystal structure of ZnO, was presented in all synthesized nanocrystals. The inset in Fig. 5 shows that $E_2^{(high)}$ mode only slightly shifts to higher frequencies with the increase of Mg content indicating the almost constant vibrations of oxygen atoms [57]. On the other hand, such small shift can signal about the stress coming from the doping-related defects which disorder the lattice [58].

As Mg doping level increases up to 5 at.%, an additional mode at 392 cm^{-1} appears which could be assigned to E_u(TO) mode of $Mg(OH)_2$ [59,60]. Also, considering the most intense $E_2^{(high)}$ mode, its intensity decreases and FWHM increases, indicating the worsening of the crystal structure quality of ZnO nanocrystals, probably due to the appearance of new defects in the host lattice. Moreover, the redshift of $E_2^{(low)}$ mode from 89 cm^{-1} to 91 cm^{-1}, as shown on the inset b in Fig. 5, suggests successful incorporation of Mg atoms into ZnO lattice.

This can be explained either by the difference of masses between Mg (24.3 amu) and Zn (65.4 amu) atoms or increased force constants in atom vibrations [61]. The mode identification and structural parameters obtained from Raman spectra of the synthesized nanocrystals are presented in Table 3. It should be noted that these results are in good agreement with XRD, TEM, SEM, EDS analyses. The transmission and absorbance spectra recorded in the UV and visible wavelength range (320–800 nm) and $(\alpha h\nu)^2$-$(h\nu)$ plot to determine the optical band gap energies of undoped and Mg-doped ZnO nanocrystals are shown in Fig. 6. Mg doping led to the shift of absorption edge to higher energies. We exclude the possible alteration of the optical band gap energies due to the quantum confinement effects referring to larger sizes of the synthesized nanocrystals compared with Bohr radius of ZnO [55].

The observed peak shifts can be explained by Burstein-Moss effect [62,63]:

$$E_g = E_g^0 + E_g^{BM}, \quad E_g^{BM} = h^2 N^{2/3}/8m_e^*\pi^{2/3}, \tag{3}$$

where h is Planck's constant, N is carrier concentration and m_e is effective mass of electrons. The values of E_g of the nanomaterials has been found to be direct falling in the range of 3.40 eV at 0 at.% up to 3.80 eV at 20 at.% (the calculation results are presented in Fig. 6c and Table 4).

The introduction of Mg ions into the unit lattice, doping induced crystal disorder and the oxygen excess as the additional source of the carriers (as shown by EDS analysis in Table 2) can be regarded as the major factors for the band gap widening. We were not able to detect any $Mg(OH)_2$ absorption peak as its band-to-band charge transition is in UV wavelength range near 230 nm which is out of the measured wavelength range [64]. The indicated band gaps are similar to values determined for Mg-doped ZnO nanocrystals synthesized by the solution-based techniques [37,39,65]. In brief, Mallika et al. [37] have pointed out that 1–5 mol.% Mg doping leads to the blue shifting of absorption peak from 377 nm (3.29 eV) to 362 nm (3.42 eV). Chandrasekaran et al. [39] have showed that for $Zn_{1-x}Mg_xO$ nanocrystals the absorption onset shifts from 363.5 nm (3.41 eV) at x = 0–359 nm (3.45 eV) at x = 0.1. In addition, Mia et al. [65] have stated that changing Mg content from 2 at.% to 8 at.% facilitates tuning bandgap energies in the range of

3.30 eV–3.39 eV. In comparison with these works, the polyol approach to obtain Mg doped ZnO nanostructures, used in this work, has allowed to control the optical band gap in the wider energy diapason.

4. Conclusions

The undoped and Mg-doped ZnO nanocrystals have been synthesized using polyol process. The effects of magnesium doping on the morphological, structural, optical properties and chemical composition of the nanomaterials have been studied for 0–20 at.% Mg concentration range. ZnO nanocrystals doped with up to 1 at.% possess the single crystal structure phase. Further increase in Mg concentration from 5 at.% up to 20 at.% leads to the appearance of $Mg(OH)_2$ secondary phase and high disorder of host ZnO lattice.

Mg doping leads to the decrease of nanocrystal size and appearance of the rod-like net and amorphous nanostructures. EDS analysis has confirmed the successful incorporation of the randomly distributed Mg ions with the small traces of Cl residuals. Raman spectroscopy has allowed to identify the hexagonal crystal structure of ZnO nanomaterials. Doping at 5 at.% has led to the appearance of $Mg(OH)_2$ secondary phase confirming XRD results.

The optical band gap of ZnO nanocrystals has been found to be direct falling in range of 3.40 eV up to 3.80 eV. The similar behavior of nanoparticles size reduction, lowering the crystal structure quality and appearance of $Mg(OH)_2$ secondary phase in ZnO nanocrystals doped with Mg ions and prepared by solution-based methods have been also shown by the several other works [34,35,37,38].

Acknowledgments

The present work is supported by Ministry of Education and Science of Ukraine (grant number 0116U002619) and Ukrainian-Lithuanian R&D Project (grant number M/80-2018). O.D. thanks to National Scholarship Programme of the Slovak Republic (SAIA) for his research stay grant at Institute of Geotechnics of Slovak Academy of Sciences. P.B. thanks to the Slovak Research and Development Agency APVV (project VV-0357-18) for support of this work. The authors declare no conflict of interest.

Appendix A. Supplementary data

Supplementary data to this article can be found online at https://doi.org/10.1016/j.mssp.2019.104595.

References

[1] Ü. Özgür, Y.I. Alivov, C. Liu, A. Teke, M.A. Reshchikov, S. Doğan, V. Avrutin, S.-J. Cho, H. Morkoç, A comprehensive review of ZnO materials and devices, J. Appl. Phys. 98 (4) (2005) 041301 https://dx.doi.org/10.1063/1.1992666.
[2] J. Wang, R. Chen, L. Xiang, S. Komarneni, Synthesis, properties and applications of ZnO nanomaterials with oxygen vacancies: a review, Ceram. Int. 44 (7) (2018) 7357–7377 https://dx.doi.org/10.1016/j.ceramint.2018.02.013.
[3] C.B. Ong, L.Y. Ng, A.W. Mohammad, A review of ZnO nanoparticles as solar photocatalysts: synthesis, mechanisms and applications, Renew. Sustain. Energy Rev. 81 (2018) 536–551 https://dx.doi.org/10.1016/j.rser.2017.08.020.
[4] M. Law, L.E. Greene, J.C. Johnson, R. Saykally, P. Yang, Nanowire dye-sensitized solar cells, Nat. Mater. 4 (2005) 455 https://dx.doi.org/10.1038/nmat1387.
[5] M. Hosni, Y. Kusumawati, S. Farhat, N. Jouini, T. Pauporté, Effects of oxide nanoparticle size and shape on electronic structure, charge transport, and recombination in dye-sensitized solar cell photoelectrodes, J. Phys. Chem. C 118 (30) (2014) 16791–16798 https://dx.doi.org/10.1021/jp412772b.
[6] Y.-Z. Zheng, X. Tao, Q. Hou, D.-T. Wang, W.-L. Zhou, J.-F. Chen, Iodine-doped ZnO nanocrystalline aggregates for improved dye-sensitized solar cells, Chem. Mater. 23 (1) (2011) 3–5 https://dx.doi.org/10.1021/cm101525p.
[7] J. Kwak, W.K. Bae, D. Lee, I. Park, J. Lim, M. Park, H. Cho, H. Woo, D.Y. Yoon, K. Char, S. Lee, C. Lee, Bright and efficient full-color colloidal quantum dot light-emitting diodes using an inverted device structure, Nano Lett. 12 (5) (2012) 2362–2366 https://dx.doi.org/10.1021/nl3003254.
[8] P. Jood, R.J. Mehta, Y. Zhang, G. Peleckis, X. Wang, R.W. Siegel, T. Borca-Tasciuc, S.X. Dou, G. Ramanath, Al-doped zinc oxide nanocomposites with enhanced thermoelectric properties, Nano Lett. 11 (10) (2011) 4337–4342 https://dx.doi.org/10.1021/nl202439h.
[9] A. McLaren, T. Valdes-Solis, G. Li, S.C. Tsang, Shape and size effects of ZnO nanocrystals on photocatalytic activity, J. Am. Chem. Soc. 131 (35) (2009) 12540–12541 https://dx.doi.org/10.1021/ja9052703.
[10] B. Liu, J. Xu, S. Ran, Z. Wang, D. Chen, G. Shen, High-performance photodetectors, photocatalysts, and gas sensors based on polyol reflux synthesized porous ZnO nanosheets, CrystEngComm 14 (14) (2012) 4582–4588 https://dx.doi.org/10.1039/C2CE25278C.
[11] Z. Jia, R.D.K. Misra, Tunable ZnO quantum dots for bioimaging: synthesis and photoluminescence, Mater. Technol. 28 (4) (2013) 221–227 https://dx.doi.org/10.1179/1753555713Y.0000000061.
[12] X. Tang, E.S.G. Choo, L. Li, J. Ding, J. Xue, One-pot synthesis of water-stable ZnO nanoparticles via a polyol hydrolysis route and their cell labeling applications, Langmuir 25 (9) (2009) 5271–5275 https://dx.doi.org/10.1021/la900374b.
[13] L.-H. Zhao, S.-Q. Sun, Synthesis of water-soluble ZnO nanocrystals with strong blue emission via a polyol hydrolysis route, CrystEngComm 13 (6) (2011) 1864–1869 https://dx.doi.org/10.1039/C0CE00548G.
[14] A. Anžlovar, K. Kogej, Z.C. Orel, M. Žigon, Impact of inorganic hydroxides on ZnO nanoparticle formation and morphology, Cryst. Growth Des. 14 (9) (2014) 4262–4269 https://dx.doi.org/10.1021/cg401870e.
[15] I. Trenque, S. Mornet, E. Duguet, M. Gaudon, New insights into crystallite size and cell parameters correlation for ZnO nanoparticles obtained from polyol-mediated synthesis, Inorg. Chem. 52 (21) (2013) 12811–12817 https://dx.doi.org/10.1021/ic402152f.
[16] M. Wang, A.-D. Li, J.-Z. Kong, Y.-P. Gong, C. Zhao, Y.-F. Tang, D. Wu, Fabrication and characterization of ZnO nano-clips by the polyol-mediated process, Nanoscale Res. Lett. 13 (1) (2018) 47 https://dx.doi.org/10.1186/s11671-018-2458-9.
[17] C. Feldmann, Polyol-mediated synthesis of nanoscale functional materials, Solid State Sci. 7 (7) (2005) 868–873 https://dx.doi.org/10.1016/j.solidstatesciences.2005.01.018.
[18] S. Lee, S. Jeong, D. Kim, S. Hwang, M. Jeon, J. Moon, ZnO nanoparticles with controlled shapes and sizes prepared using a simple polyol synthesis, Superlattice. Microst. 43 (4) (2008) 330–339 https://dx.doi.org/10.1016/j.spmi.2008.01.004.
[19] B.W. Chieng, Y.Y. Loo, Synthesis of ZnO nanoparticles by modified polyol method, Mater. Lett. 73 (2012) 78–82 https://dx.doi.org/10.1016/j.matlet.2012.01.004.
[20] T.E.P. Alves, C. Kolodziej, C. Burda, A. Franco, Effect of particle shape and size on the morphology and optical properties of zinc oxide synthesized by the polyol method, Mater. Des. 146 (2018) 125–133 https://dx.doi.org/10.1016/j.matdes.2018.03.013.
[21] R. Yogamalar, S. Anitha, R. Srinivasan, A. Vinu, K. Ariga, A.C. Bose, An investigation on co-precipitation derived ZnO nanospheres, J. Nanosci. Nanotechnol. 9 (10) (2009) 5966–5972 https://dx.doi.org/10.1166/jnn.2009.1289.
[22] T. Andelman, Y. Gong, M. Polking, M. Yin, I. Kuskovsky, G. Neumark, S. O'Brien, Morphological control and photoluminescence of zinc oxide nanocrystals, J. Phys. Chem. B 109 (30) (2005) 14314–14318 https://dx.doi.org/10.1021/jp050540o.
[23] J.M. Hodges, J.L. Fenton, J.L. Gray, R.E. Schaak, Colloidal ZnO and $Zn_{1-x}Co_xO$ tetrapod nanocrystals with tunable arm lengths, Nanoscale 7 (40) (2015) 16671–16676 https://dx.doi.org/10.1039/C5NR04425A.
[24] Y. Zheng, C. Chen, Y. Zhan, X. Lin, Q. Zheng, K. Wei, J. Zhu, Y. Zhu, Luminescence and photocatalytic activity of ZnO nanocrystals: correlation between structure and property, Inorg. Chem. 46 (16) (2007) 6675–6682 https://dx.doi.org/10.1021/ic062394m.
[25] D. Sridev, K.V. Rajendran, Synthesis and optical characteristics of ZnO nanocrystals, Bull. Mater. Sci. 32 (2) (2009) 165–168 https://dx.doi.org/10.1007/s12034-009-0025-9.
[26] S. Rani, P. Suri, P.K. Shishodia, R.M. Mehra, Synthesis of nanocrystalline ZnO powder via sol-gel route for dye-sensitized solar cells, Sol. Energy Mater. Sol. Cells 92 (12) (2008) 1639–1645 https://dx.doi.org/10.1016/j.solmat.2008.07.015.
[27] D.Y. Inamdar, S.R. Vaidya, S. Mahamuni, On the photoluminescence emission of ZnO nanocrystals, J. Exp. Nanosci. 9 (5) (2014) 533–540 https://dx.doi.org/10.1080/17458080.2012.676678.
[28] F. Xiu, J. Xu, P.C. Joshi, C.A. Bridges, M. Parans Paranthaman, ZnO doping and defect engineering - a review, in: M.P. Paranthaman, W. Wong-Ng, R.N. Bhattacharya (Eds.), Semiconductor Materials for Solar Photovoltaic Cells, Springer International Publishing, Cham, 2016, pp. 105–140 https://dx.doi.org/10.1007/978-3-319-20331-7_4.
[29] S.Y. Park, B.J. Kim, K. Kim, M.S. Kang, K.-H. Lim, T.I. Lee, J.M. Myoung, H.K. Baik, J.H. Cho, Y.S. Kim, Low-temperature, solution-processed and alkali metal doped ZnO for high-performance thin-film transistors, Adv. Mater. 24 (6) (2012) 834–838 https://dx.doi.org/10.1002/adma.201103173.
[30] O.E. Taurian, M. Springborg, N.E. Christensen, Self-consistent electronic structures of MgO and SrO, Solid State Commun. 55 (4) (1985) 351–355 https://dx.doi.org/10.1016/0038-1098(85)90622-2.
[31] R.D. Shannon, Revised effective ionic radii and systematic studies of interatomic distances in halides and chalcogenides, Acta Crystallogr. A 32 (5) (1976) 751–767 https://dx.doi.org/10.1107/S0567739476001551.
[32] S. Sundar Manoharan, S. Arora, Photoluminescent properties of Mg doped ZnO by microwave combustion and microwave polyol method, J. Mater. Sci. Eng. B 162 (1) (2009) 68–73 https://dx.doi.org/10.1016/j.mseb.2009.02.004.
[33] M. Perez-Altamar, H. Marrero, M. Martínez Julca, O. Perales Perez, Study of bactericidal properties of Mg-doped ZnO nanoparticles, MRS Proc. 1804 (2015) 31–36 https://dx.doi.org/10.1557/opl.2015.543.
[34] A.W. Cohn, K.R. Kittilstved, D.R. Gamelin, Tuning the potentials of "extra" electrons in colloidal n-type ZnO nanocrystals via Mg^{2+} substitution, J. Am. Chem. Soc. 134 (18) (2012) 7937–7943 https://dx.doi.org/10.1021/ja3019934.
[35] K. Youngjun, Y. Heesun, P. Byoungnam, Field-effect-induced transport properties of

$Zn_{1-x}Mg_xO$ nanocrystal solid solution, J. Phys. D Appl. Phys. 50 (27) (2017) 275302 https://dx.doi.org/10.1088/1361-6463/aa715d.
[36] K. Sowri Babu, A. Ramachandra Reddy, K. Venugopal Reddy, Green emission from ZnO-MgO nanocomposite due to Mg diffusion at the interface, J. Lumin. 158 (2015) 306–312 https://dx.doi.org/10.1016/j.jlumin.2014.10.027.
[37] A.N. Mallika, A. Ramachandra Reddy, K. Sowri Babu, C. Sujatha, K. Venugopal Reddy, Structural and photoluminescence properties of Mg substituted ZnO nanoparticles, Opt. Mater. 36 (5) (2014) 879–884 https://dx.doi.org/10.1016/j.optmat.2013.12.015.
[38] J.H. Li, Y.C. Liu, C.L. Shao, X.T. Zhang, D.Z. Shen, Y.M. Lu, J.Y. Zhang, X.W. Fan, Effects of thermal annealing on the structural and optical properties of $Mg_xZn_{1-x}O$ nanocrystals, J. Colloid Interface Sci. 283 (2) (2005) 513–517 https://dx.doi.org/10.1016/j.jcis.2004.09.011.
[39] P. Chandrasekaran, P. Anandan, N. Srinivasan, Structural and optical properties of sol-gel synthesised $Zn_{1-x}Mg_xO$ nanocrystals, Spectrochim. Acta, Part A 116 (2013) 311–316 https://dx.doi.org/10.1016/j.saa.2013.07.031.
[40] C. Abed, C. Bouzidi, H. Elhouichet, B. Gelloz, M. Ferid, Mg doping induced high structural quality of sol-gel ZnO nanocrystals: application in photocatalysis, Appl. Surf. Sci. 349 (2015) 855–863 https://dx.doi.org/10.1016/j.apsusc.2015.05.078.
[41] J. Lv, Q. Zhu, Z. Zeng, M. Zhang, J. Yang, M. Zhao, W. Wang, Y. Cheng, G. He, Z. Sun, Enhanced photocurrent and photocatalytic properties of porous ZnO thin film by Ag nanoparticles, J. Phys. Chem. Solids 111 (2017) 104–109 https://dx.doi.org/10.1016/j.jpcs.2017.07.017.
[42] M. Zhao, Y. Sun, J. Lv, L. Cao, Y. Jiang, G. He, M. Zhang, Z. Sun, X. Chen, Enhanced photocatalytic performances of ZnO with Na doping and graphene oxide quantum dots, J. Mater. Sci. Mater. Electron. 27 (9) (2016) 9131–9135 https://dx.doi.org/10.1007/s10854-016-4948-9.
[43] J. Lv, J. Xu, M. Zhao, P. Yan, S. Mao, F. Shang, G. He, M. Zhang, Z. Sun, Effect of seed layer on optical properties and visible photoresponse of ZnO/Cu_2O composite thin films, Ceram. Int. 41 (10) (2015) 13983–13987 https://dx.doi.org/10.1016/j.ceramint.2015.07.010.
[44] J. Lv, P. Yan, M. Zhao, Y. Sun, F. Shang, G. He, M. Zhang, Z. Sun, Effect of ammonia on morphology, wettability and photoresponse of ZnO nanorods grown by hydrothermal method, J. Alloy. Comp. 648 (2015) 676–680 https://dx.doi.org/10.1016/j.jallcom.2015.07.068.
[45] J. Lv, Y. Sun, M. Zhao, L. Cao, J. Xu, G. He, M. Zhang, Z. Sun, Rectifying properties of ZnO thin films deposited on FTO by electrodeposition technique, Appl. Surf. Sci. 366 (2016) 348–352 https://dx.doi.org/10.1016/j.apsusc.2016.01.104.
[46] D. Nam, A.S. Opanasyuk, P.V. Koval, A.G. Ponomarev, A.R. Jeong, G.Y. Kim, W. Jo, H. Cheong, Composition variations in $Cu_2ZnSnSe_4$ thin films analyzed by X-ray diffraction, energy dispersive X-ray spectroscopy, particle induced X-ray emission, photoluminescence, and Raman spectroscopy, Thin Solid Films 562 (2014) 109–113 https://dx.doi.org/10.1016/j.tsf.2014.03.079.
[47] D. Kurbatov, A. Opanasyuk, S.M. Duvanov, A.G. Balogh, H. Khlyap, Growth kinetics and stoichiometry of ZnS films obtained by close-spaced vacuum sublimation technique, Solid State Sci. 13 (5) (2011) 1068–1071 https://dx.doi.org/10.1016/j.solidstatesciences.2011.01.017.
[48] A.K. Chatterjee, X-ray diffraction, in: V.S. Ramachandran, J.J. Beaudoin (Eds.), Handbook of Analytical Techniques in Concrete Science and Technology, William Andrew Publishing, Norwich, NY, 2001, pp. 275–332 https://dx.doi.org/10.1016/B978-081551437-4.50011-4.
[49] B.E. Warren, X-ray Diffraction, Dover Publications New York, 1990, https://dx.doi.org/10.1107/S0567739471000445.
[50] O. Dobrozhan, A. Opanasyuk, M. Kolesnyk, M. Demydenko, H. Cheong, Substructural investigations, Raman, and FTIR spectroscopies of nanocrystalline ZnO films deposited by pulsed spray pyrolysis, Phys. Status Solidi A 212 (12) (2015) 2915–2921 https://dx.doi.org/10.1002/pssa.201532324.
[51] O. Dobrozhan, D. Kurbatov, A. Opanasyuk, H. Cheong, A. Cabot, Influence of substrate temperature on the structural and optical properties of crystalline ZnO films obtained by pulsed spray pyrolysis, Surf. Interface Anal. 47 (5) (2015) 601–606 https://dx.doi.org/10.1002/sia.5752.
[52] D. Shreiber, W.A. Jesser, Size dependence of lattice parameter for Si_xGe_{1-x} nanoparticles, Surf. Sci. 600 (19) (2006) 4584–4590 https://dx.doi.org/10.1016/j.susc.2006.07.026.
[53] P.M. Diehm, P. Ágoston, K. Albe, Size-dependent lattice expansion in nanoparticles: reality or anomaly? ChemPhysChem 13 (10) (2012) 2443–2454 https://dx.doi.org/10.1002/cphc.201200257.
[54] E.R. Segnit, A.E. Holland, The system MgO-ZnO-SiO_2, J. Am. Ceram. Soc. 48 (8) (1965) 409–413 https://dx.doi.org/10.1111/j.1151-2916.1965.tb14778.x.
[55] Y.-S. Fu, X.-W. Du, S.A. Kulinich, J.-S. Qiu, W.-J. Qin, R. Li, J. Sun, J. Liu, Stable aqueous dispersion of ZnO quantum dots with strong blue emission via simple solution route, J. Am. Chem. Soc. 129 (51) (2007) 16029–16033 https://dx.doi.org/10.1021/ja075604i.
[56] F. Decremps, J. Pellicer-Porres, A.M. Saitta, J.-C. Chervin, A. Polian, High-pressure Raman spectroscopy study of wurtzite ZnO, Phys. Rev. B 65 (9) (2002) 092101 https://dx.doi.org/10.1103/PhysRevB.65.092101.
[57] Y.-I. Kim, K. Page, A.M. Limarga, D.R. Clarke, R. Seshadri, Evolution of local structures in polycrystalline $Zn_{1-x}Mg_xO$ ($0 < x < 0.15$) studied by Raman spectroscopy and synchrotron x-ray pair-distribution-function analysis, Phys. Rev. B 76 (11) (2007) 115204 https://dx.doi.org/10.1103/PhysRevB.76.115204.
[58] C.A. Arguello, D.L. Rousseau, S.P.S. Porto, First-order Raman effect in wurtzite-type crystals, Phys. Rev. B 181 (3) (1969) 1351–1363 https://dx.doi.org/10.1103/PhysRev.181.1351.
[59] R.A. Buchanan, H.H. Caspers, J. Murphy, Lattice vibration spectra of $Mg(OH)_2$ and $Ca(OH)_2$, Appl. Opt. 2 (11) (1963) 1147–1150 https://dx.doi.org/10.1364/AO.2.001147.
[60] F. Pascale, S. Tosoni, C. Zicovich-Wilson, P. Ugliengo, R. Orlando, R. Dovesi, Vibrational spectrum of brucite, $Mg(OH)_2$: a periodic ab initio quantum mechanical calculation including OH anharmonicity, Chem. Phys. Lett. 396 (4) (2004) 308–315 https://dx.doi.org/10.1016/j.cplett.2004.08.047.
[61] Z.-Y. Jiang, K.-R. Zhu, Z.-Q. Lin, S.-W. Jin, G. Li, Structure and Raman scattering of Mg-doped ZnO nanoparticles prepared by sol-gel method, Rare Met. 37 (10) (2018) 881–885 https://dx.doi.org/10.1007/s12598-015-0505-6.
[62] B.E. Sernelius, K.F. Berggren, Z.C. Jin, I. Hamberg, C.G. Granqvist, Band-gap tailoring of ZnO by means of heavy Al doping, Phys. Rev. B 37 (17) (1988) 10244–10248 https://dx.doi.org/10.1103/PhysRevB.37.10244.
[63] A. Sarkar, S. Ghosh, S. Chaudhuri, A.K. Pal, Studies on electron transport properties and the Burstein-Moss shift in indium-doped ZnO films, Thin Solid Films 204 (2) (1991) 255–264 https://dx.doi.org/10.1016/0040-6090(91)90067-8.
[64] R. Bhargava, S. Khan, Effect of reduced graphene oxide (rGO) on structural, optical, and dielectric properties of $Mg(OH)_2$/rGO nanocomposites, Adv. Powder Technol. 28 (11) (2017) 2812–2819 https://dx.doi.org/10.1016/j.apt.2017.08.008.
[65] M.N.H. Mia, M.F. Pervez, M.K. Hossain, M. Reefaz Rahman, M.J. Uddin, M.A. Al Mashud, H.K. Ghosh, M. Hoq, Influence of Mg content on tailoring optical bandgap of Mg-doped ZnO thin film prepared by sol-gel method, Results Phys. 7 (2017) 2683–2691 https://dx.doi.org/10.1016/j.rinp.2017.07.047.